Journal of Mathematical Chemistry 20 (1996) 213–233 

# Travelling waves in an open cubic autocatalytic system

M.A. Sadiq and J.H. Merkin

*Department of Applied Mathematical Studies, University of Leeds, Leeds LS2 9JT, UK*

Received 30 May 1996; revised 7 November 1996

A continuous-flow, unstirred reactor (CFUR) is considered in which the reaction is purely cubic autocatalysis and in which the exchange of reactants between the reactor and its reservoir is modelled by linear diffusive interchange terms. The system is capable of supporting two, stable, spatially uniform stationary states. The possibilities of initiating travelling waves of permanent form (front waves), in which the concentrations vary monotonically between these two stationary states is, investigated. It is seen that the formation of front waves requires the dimensionless parameter $\delta = D_A/D_B$ ($D_A$, $D_B$ being the diffusion coefficients of reactant and autocatalyst, respectively) to be such that $\delta \lesssim 4$, a result confirmed by numerical integrations of an initial-value problem. For values of $\delta$ larger than this, permanent-form waves are not initiated with a more complex structure evolving in the initial-value problem. Here the forward-propagating front leaves behind a region in which oscillations in the concentrations of both species are observed. These individual oscillations are spatially fixed with the region where this oscillatory response is observed propagating backwards into the region of spatially uniform concentration.

## 1. Introduction

Travelling waves of reaction form the basis of many complex chemical and biological processes and consequently have received considerable attention. One way of studying reaction-diffusion waves experimentally is through the continuous-flow, unstirred reactor (CFUR). This is an arrangement whereby a continuous supply of reactants can be fed into the system, in a way that does not interfer with the transport processes by molecular diffusion. A reaction zone, which is usually a gelled medium, is contained within impermeable walls at its ends but is also in contact with a reservoir from which fresh reactant can be exchanged and into which reaction products can be removed. The composition of the reservoir can be kept constant by continuous flow, for example, thus enabling steady states and other reaction-diffusion structures to be maintained indefinitely.

Here we consider a situation in which the reaction within the CFUR is isothermal and given by purely cubic autocatalytic kinetics, represented by

$$A + 2B \rightarrow 3B, \quad \text{rate } kab^2, \tag{1}$$

where $a$ and $b$ are the concentrations of chemical species $A$ and $B$, respectively, and $k$ is the rate constant. We also assume that the reservoir contains reactant $A$ and autocatalyst $B$ at the constant concentrations $a_0$ and $b_0$ respectively, with the exchange between reactor and reservoir given by linear diffusive interchange, with the associated mass transfer coefficient $m_R$. Finally, we take the reactor to be long relative to its width, enabling us to limit attention to one space dimension, along the length of the reactor, and, in our discussion of the travelling waves that arise in this system, for the effects of the ends of the reactor to be neglected.

The equations describing the reaction and diffusion processes for our model of the CFUR are then

$$\frac{\partial a}{\partial t} = D_A \frac{\partial^2 a}{\partial x^2} + m_R(a_0 - a) - kab^2, \tag{2}$$

$$\frac{\partial b}{\partial t} = D_B \frac{\partial^2 b}{\partial x^2} + m_R(b_0 - b) + kab^2, \tag{3}$$

where $D_A$ and $D_B$ are the diffusion coefficients of reactant $A$ and autocatalyst $B$, respectively. To transform eqs. (2), (3) into a simpler form, we introduce the dimensionless variables variables

$$a = a_0\bar{a}, \quad b = a_0\bar{b}, \quad \bar{x} = \left(\frac{ka_0^2}{D_B}\right)^{1/2} x, \quad \bar{t} = (ka_0^2)t. \tag{4}$$

Applying (4) to eqs. (2), (3) gives, on dropping the bars for convenience,

$$\frac{\partial a}{\partial t} = \delta \frac{\partial^2 a}{\partial x^2} + \mu(1 - a) - ab^2, \tag{5}$$

$$\frac{\partial b}{\partial t} = \frac{\partial^2 b}{\partial x^2} + \mu(\beta_0 - b) + ab^2, \tag{6}$$

where the dimensionless parameters are $\delta = D_A/D_B$, $\mu = m_R/ka_0^2$ and $\beta_0 = b_0/a_0$.

Eqs. (5), (6), augmented by the linear termination step $B \rightarrow C$ (giving the full Gray–Scott kinetic model), or, equivalently, taking different mass transfer coefficients for $A$ and $B$, is essentially the system studied by Pearson and co-workers [1–3], Petrov et al. [4], Merkin et al. [5,6] and Merkin and Sadiq [7]. This augmented system has been shown to display a very wide range of complex spatio-temporal behaviour, including wave and spot replication and extinction [1–3], wave reflection at boundaries and wave splitting [4] and travelling wave-induced spatio-temporal chaos [5–7]. This behaviour stems essentially from the fact that the system is capable of sustaining three spatially uniform stationary states, one of which can change its stability (through a Hopf bifurcation) with the other two remaining stable and unstable respectively. Here the situation is somewhat simpler. The sys-

tem given by eqs. (5), (6) can still have up to three spatially uniform stationary states, but now two of these remain stable (nodes) while the other is always unstable (saddle) for all the parameter values for which they exist. (Where there is just one stationary state this is also stable for all parameter values.)

The implications of this for the reaction-diffusion system (5), (6) is that any travelling waves of permanent form that arise can be purely front (or autocatalytic) waves, in which the reacting medium is converted from one (stable) stationary state at its front to the other (stable) stationary state at its rear. It is the existence of these travelling fronts that we concentrate mainly on in this paper. We establish that there is an upper bound on $\delta$ ($\delta_1$, say) for the existence of these simple front waves. We then examine the consequences of this for wave initiation by obtaining numerical solutions to an initial-value problem. These show that when $\delta < \delta_1$, simple front waves evolve, the direction of propagation of which depends on the parameters $\mu$ and $\beta_0$ and (weakly) on $\delta$. When $\delta > \delta_1$, a, perhaps unexpected, complex wave structure evolves. In this case there is still a propagating front (similar in form to that found for $\delta < \delta_1$) but now there is also an expanding region behind this front in which the concentrations undergo (in some cases quite large) oscillatory responses which remain fixed in space. We start with a brief review of the kinetics of eqs. (5), (6).

## 2. Kinetics

The kinetics for eqs. (5), (6) are given by the ordinary differential equations

$$\dot{a} = \mu(1 - a) - ab^2 , \tag{7}$$

$$\dot{b} = \mu(\beta_0 - b) + ab^2 \tag{8}$$

in $a, b \geqslant 0$, with $\mu \geqslant 0$, $\beta_0 \geqslant 0$. Eqs. (7), (8) are discussed in detail by Gray and Scott [8] where it was shown that the stationary states $(a_s, b_s)$, given by the algebraic equation

$$b_s^3 - (1 + \beta_0)b_s^2 + \mu(b_s - \beta_0) = 0 \tag{9}$$

for $b_s$ (say), undergo a hysteresis bifurcation at $\beta_0 = 1/8$, $\mu = 27/64$, $b_s = 3/8$. For $\beta_0 < 1/8$, the system can sustain three stationary states, with a typical plot of $b_s$ against $\mu$ being shown in Fig. 1(a). The upper and lower solution branches $b_3$ and $b_1$, respectively, (with corresponding stationary states for $A$ of $a_3$ and $a_1$) are both stable (nodes), while the middle branch is unstable (saddle-point) in all cases. The region of $(\beta_0, \mu)$ parameter space in which these multiple solutions exist is shown in Fig. 1(b). For $\beta_0 > 1/8$, the $b_s \sim \mu$ curve is monotone (decreasing) with this single stationary state being stable (node). Finally, we note that the stationary states satisfy the inequalities, $0 \leqslant a_s \leqslant 1$, $\beta_0 \leqslant b_s \leqslant 1 + \beta_0$.

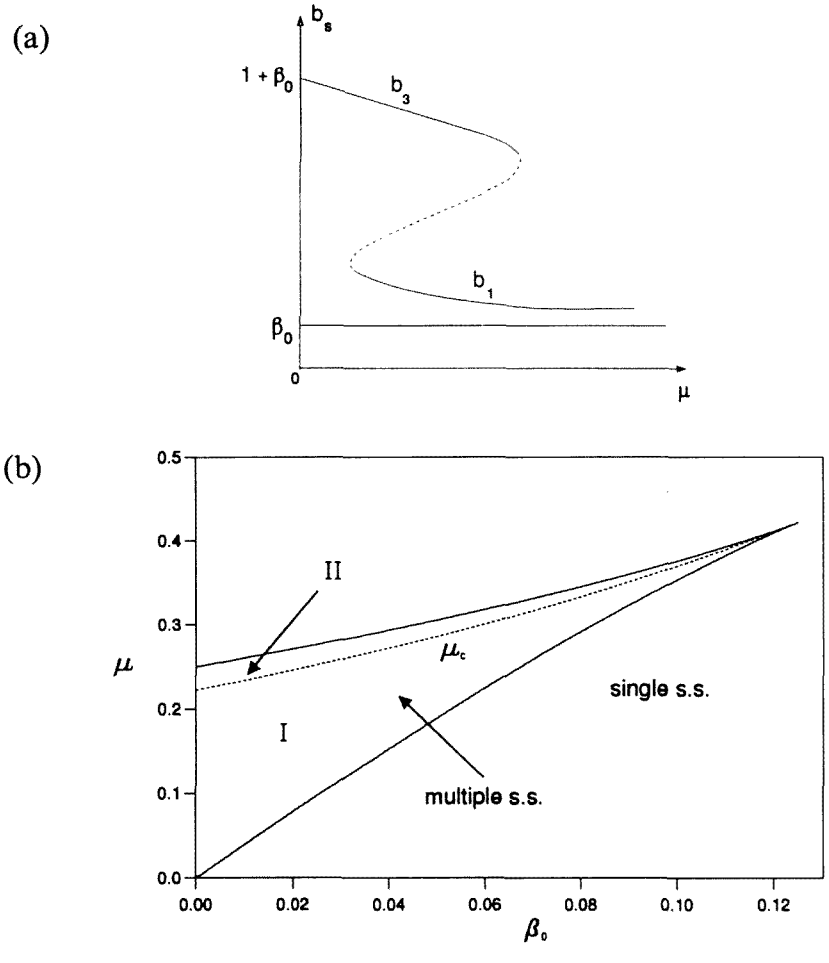


Fig. 1. (a) A plot of $b_s$ against $\mu$ for a value of $\beta_0$ in $0 < \beta_0 < 1/8$. The upper and lower solution branches are stable (indicated by the full line), the middle branch is unstable (indicated by the broken line). (b) A plot of the critical points for $\mu$ against $\beta_0$. The regions of parameter space where eq. (9) has a single stationary state, and where there are multiple stationary states are shown. Also shown (by the broken line) is a plot of $\mu_c$ against $\beta_0$ for $\delta = 1$ (where the travelling wave eqs. (12), (13) have a solution with $v = 0$). The regions where type I and type II waves are initiated are also indicated.

For $\beta_0 = 0$, the stationary states can be written down explicitly as

$$a_s = 1, \quad b_s = 0, \tag{10}$$

$$a_s = \frac{1 \mp \sqrt{1-4\mu}}{2}, \quad b_s = \frac{1 \pm \sqrt{1-4\mu}}{2}. \tag{11}$$

We now have sufficient information to discuss the travelling wave solutions to eqs. (5), (6).

## 3. Travelling waves

A travelling wave of permanent form is a non-negative, non-trivial solution to eqs. (5), (6) expressed in terms of the single travelling co-ordinate $y = x - vt$, where $v$ is the constant wave speed and where, without any loss in generality, we can take $v \geqslant 0$. The solution should also be such that conditions are uniform at both the front and the rear of the wave (i.e. as $y \to \pm\infty$). This leads us to consider the equations

$$\delta a'' + va' + \mu(1 - a) - ab^2 = 0\,, \tag{12}$$

$$b'' + vb' + \mu(\beta_0 - b) + ab^2 = 0 \tag{13}$$

subject to the boundary conditions

$$a \to a_1, \quad b \to b_1 \quad \text{as } y \to \infty;$$

$$a \to a_3, \quad b \to b_3 \quad \text{as } y \to -\infty\,, \tag{14}$$

or

$$a \to a_3, \quad b \to b_3 \quad \text{as } y \to \infty;$$

$$a \to a_1, \quad b \to b_1 \quad \text{as } y \to -\infty\,, \tag{15}$$

where, from above, $b_3 > b_1$. We will refer to waves which satisfy boundary conditions (14) as type I waves, and waves which satisfy boundary conditions (15) as type II waves. These are illustrated in Fig. 2. There is also the possibility of pulse waves, which are waves which attain the same conditions at both front and rear, i.e. which satisfy

$$a \to a_i, \quad b \to b_i \quad \text{as } |y| \to \infty \quad (i = 1 \text{ or } 3)\,. \tag{16}$$

We start by noting that, when $\mu = 0$, eqs. (12, 13) reduce to the standard cubic-Fisher problem, see, for example, [9–11]. For $\delta = 1$, the equations have a simple solution [9,11] with wave speed $v = 1/\sqrt{2}$. For $\delta \neq 1$, the equations have to be solved numerically with results being given in [10] (where an extensive discussion of the behaviour of the solution is also given).

We are also able to establish the result that

$$a(y) \leqslant 1, \quad b(y) \geqslant \beta_0, \quad -\infty < y < \infty\,. \tag{17}$$

To do so we assume the contrary, i.e. there is some range of $y$ over which $a(y) > 1$. The boundary conditions then imply that there must be (at least) one point, $y_0$ (*say*) on this range at which $a$ takes a local maximum, with then

$$a(y_0) > 1, \quad a'(y_0) = 0, \quad a''(y_0) \leqslant 0\,.$$

However, eq. (12) gives

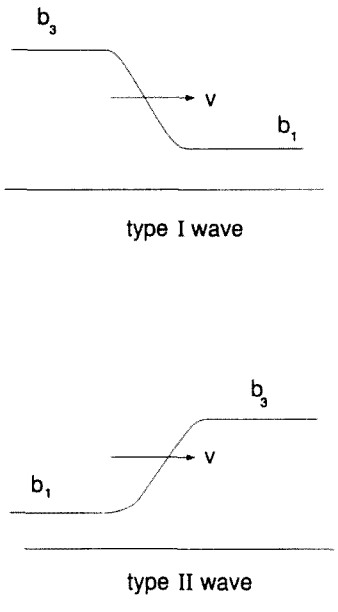


Fig. 2. A schematic representation of type I and type II waves.

$$\delta a''(y_0) = \mu(a(y_0) - 1) + a(y_0)b(y_0)^2 > 0\,,$$

which gives the contradiction. The inequality for $b(y)$ can be established in a similar way.

We start by considering the case when $\delta = 1$ (i.e. $D_B = D_A$) for which travelling wave equations can be simplified.

(a) $\delta = 1$, $D_B = D_A$

When eqs. (12), (13) with $\delta = 1$ are added, then by considering the resulting equation subject to boundary conditions (14) or (15), it is straightforward to show that

$$a + b \equiv 1 + \beta_0\,. \tag{18}$$

Using (18) eq. (13) becomes

$$b'' + vb' + \mu(\beta_0 - b) + (1 + \beta_0 - b)b^2 = 0\,. \tag{19}$$

If we now multiply eq. (19) by $b'$ and integrate, we obtain

$$v\int_{-\infty}^{\infty} b'^2\,dy = \left[\frac{b}{12}(3b^3 - 4(1 + \beta_0)b^2 + 6\mu b - 12\mu\beta_0)\right]_{b_s}^{b_s}, \tag{20}$$

where $b_s$ represents either $b_1$ or $b_3$. Eq. (20) shows that we cannot have pulse waves in this case.

For type I waves we then require

$$(b_1 - b_3)F(b_1, b_3; \mu, \beta_0) > 0\,, \tag{21}$$

where the function

$$F(b_1, b_3; \mu, \beta_0) = 3(b_1 + b_3)(b_1^2 + b_3^2) - 4(1 + \beta_0)(b_1^2 + b_1 b_3 + b_3^2) + 6\mu(b_1 + b_3) - 12\mu\beta_0$$

is symmetric in $b_1$ and $b_3$. Hence for type I waves we require $F < 0$, whereas for type II waves, we must have $F > 0$. We can then expect a curve in $\mu \sim \beta_0$ parameter space $\mu = \mu_c(\beta_0)$, (say) which divides the region of existence of multiple stationary states into regions where type I and type II waves exist. This will correspond to $F = 0$, i.e. to stationary waves, which are solutions of eq. (19) with $v = 0$. For general values of $\beta_0$ and $\mu$, the calculation of this curve has to be done numerically (as we do not have explicit expressions for the $b_s$). This is straightforward to do and a graph of $\mu_c$, plotted against $\beta_0$, is also shown in Fig. 1(b), the regions of existence of type I and type II waves are indicated in this figure.

When there is no $B$ in the reservoir i.e. $\beta_0 = 0$, the solution to eq. (19) can be expressed in the form

$$b' = \frac{\sqrt{2}}{4} b(2b - (1 + \sqrt{1 - 4\mu})), \quad v = \frac{\sqrt{2}}{4}(3\sqrt{1 - 4\mu} - 1) \tag{22}$$

for type I waves (with obvious changes in sign for type II waves). This then gives a value of $\mu_c = 2/9$ (where $v = 0$) in this case, with type I waves for $0 \leqslant \mu < 2/9$, and type II waves for $2/9 < \mu < 1/4$.

(b) *General case*

We have identified that there is a value of $\mu = \mu_c$, at which the travelling wave equations have a solution with $v = 0$, which divides the parameter space up into regions where type I and type II wave exist (both with $v > 0$). For general values of the parameters this has to be found numerically and the results for $\beta_0 = 0$ are shown in Fig. 3. From this figure, we can see that there is an upper bound on $\delta$, $\delta_1$ (say) for both types of waves exist. For $\delta > \delta_1$, stationary waves (i.e. waves with $v = 0$) cannot be formed. We will return below to the question of the nature of the solution for $\delta > \delta_1$. For $\beta_0 = 0$, we find that $\delta_1 \simeq 4.006$. (Note that the existence of multiple solutions requires $\mu < 1/4$ in this case).

Further insights into what types of waves can be initiated are provided by solutions to eqs. (12), (13) valid for $\delta \ll 1$ and $\beta_0 \simeq 1/8$ (close to the point where there is a hysteresis bifurcation in the stationary states). We start with the former case

(c) *Solution for $\delta \ll 1$, i.e. $D_A \ll D_B$*

To obtain a solution of eqs. (12), (13) valid for $\delta \ll 1$, we look for a solution by directly expanding

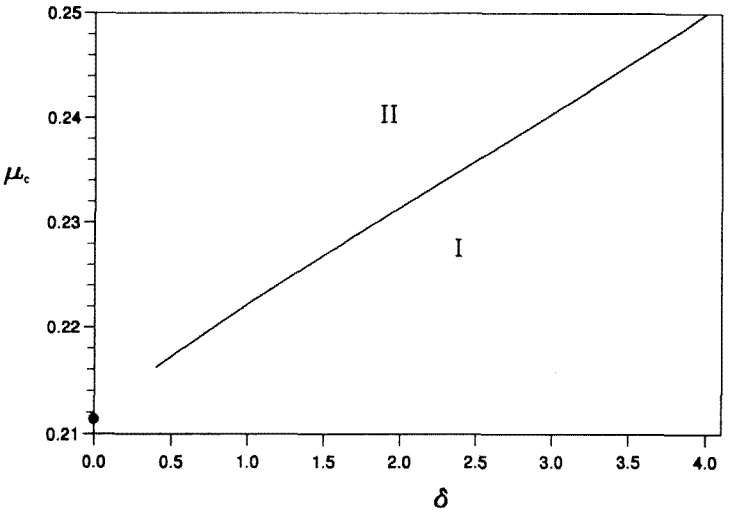


Fig. 3. $\mu_c$ plotted against $\delta$ for $\beta_0 = 0.0$ ($\mu_c$ is the value of $\mu$ at which the travelling wave equations have a solution with $v = 0$). The regions of $\mu \sim \delta$ parameter space where type I and type II waves are initiated are indicated. ● denotes the value calculated for the case $\delta = 0.0$.

$$a(y;\delta) = a_0(y) + \delta a_1(y) + \dots ,$$

$$b(y;\delta) = b_0(y) + \delta b_1(y) + \dots ,$$

$$v = v_0 + \delta v_1 + \dots . \tag{23}$$

At leading order, we obtain

$$v_0 a_0' + \mu(1 - a_0) - a_0 b_0^2 = 0 , \tag{24}$$

$$b_0'' + v_0 b_0' + \mu(\beta_0 - b_0) + a_0 b_0^2 = 0 \tag{25}$$

subject to boundary conditions (14), (15) or (16).

The numerical solutions shown in Fig. 3 show that eqs. (24), (25) are capable of supporting both type I and type II waves. This leads us to look for the value for $\mu_c$ for $\delta$ small, i.e. to look for a solution of eqs. (24), (25) with $v_0 = 0$. In this case, eq. (24) gives $a_0 = \mu_c/(\mu_c + b_0^2)$, with eq. (25) then becoming

$$b_0'' + \frac{\mu_c b_0^2}{\mu_c + b_0^2} + \mu(\beta_0 - b_0) = 0 . \tag{26}$$

If we now multiply eq. (26) by $b_0'$, and use $b_0 \to b_1$ and $b_3$ as $b_0' \to 0$, we obtain the condition that

$$\int_{b_1}^{b_3} \left( \frac{b^2}{\mu_c + b^2} + \beta_0 - b \right) db = 0 \tag{27}$$

from which it follows that $\mu_c$ is given by the equation

$$(b_1 - b_3)[1 + \beta_0 - \tfrac{1}{2}(b_1 + b_3)] - \sqrt{\mu_c}\left[\tan^{-1}\left(\frac{b_3}{\sqrt{\mu_c}}\right) - \tan^{-1}\left(\frac{b_1}{\sqrt{\mu_c}}\right)\right] = 0 .$$

Eq. (28) gives an implicit expression for $\mu_c$ which has to be determined numerically. This is straightforward to achieve and a graph of $\mu_c$ obtained from these calculations is shown in Fig. 4. Also included in this figure are the regions of $\mu \sim \beta_0$ parameter space where type I and type II waves are initiated. Note that the values of $\mu_c$ for $\delta = 0$ are very similar to the corresponding values for $\delta = 1$ (Fig. 1(b)). This is illustrated by the fact that $\mu_c = 0.2114$ from the solution for $\delta = 0$ as compared to $\mu_c = 2/9 = 0.2222$, for $\delta = 1$.

(d) *Solution for $\beta_0 \simeq 1/8$*

The stationary states, as given by eq. (9), undergo a hysteresis bifurcation at $\beta_0 = 1/8$ (and $a_s = 3/4$, $b_s = 3/8$, $\mu = 27/64$) and here we examine the nature of the solution to the travelling wave eqs. (12), (13) close to this point. We start by first considering the nature of the stationary states close to this point and to do so we put

$$\beta_0 = \tfrac{1}{8} - \epsilon, \quad 0 < \epsilon \ll 1 , \tag{29}$$

and then

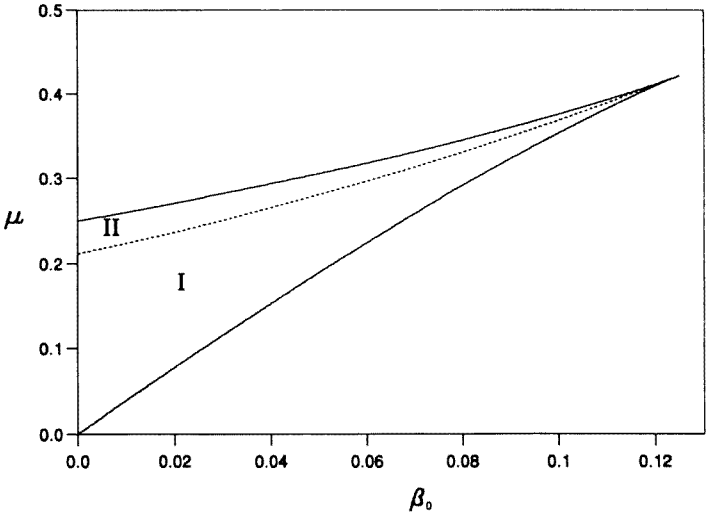


Fig. 4. $\mu_c$ plotted against $\beta_0$ for $\delta = 0.0$. The regions of $\mu \sim \beta_0$ parameter space where type I and type II waves are initiated are indicated.

$$b = \tfrac{3}{8} + \epsilon^{1/2} B, \quad \mu = \tfrac{27}{64} - \tfrac{9}{4}\epsilon + \epsilon^{3/2}\lambda . \tag{30}$$

Applying (29), (30) in eq. (9) gives the equation

$$B^3 - \tfrac{3}{2}B + \tfrac{1}{4}\lambda = 0 \tag{31}$$

at leading order. A graph $B$ plotted against $\lambda$ is shown in Fig. 5, from which we can see that there are multiple stationary states for $\lambda$ in the range $-2\sqrt{2} < \lambda < 2\sqrt{2}$ with $B$ in the range $-\sqrt{2} < B < \sqrt{2}$. From this it then follows that the curves bounding the region of multiple solutions as shown in Figs. 1(b) and 4 are given by

$$\mu \sim \tfrac{27}{64} - \tfrac{9}{4}\epsilon \pm 2\sqrt{2}\epsilon^{3/2} + \ldots \quad \text{as } \epsilon = \tfrac{1}{8} - \beta_0 \to 0 . \tag{32}$$

The above discussion suggests that to obtain a solution of the travelling wave equations valid for $\epsilon$ small, we should still apply transformations (30) as well as writing

$$\zeta = \epsilon^{1/2} y, \quad v = \epsilon^{1/2} V, \quad a = \tfrac{3}{4} + \epsilon^{1/2} A \tag{33}$$

(with $\epsilon$ still given by (29)). Using expressions (30, 33) we obtain, from eqs. (12), (13),

$$\frac{9}{16}(A+B) + \frac{3}{4}\left(AB + B^2 + \frac{3}{4}\right)\epsilon^{1/2} + \left(AB^2 - \frac{9}{4}A - \frac{\lambda}{4} - \delta A''_{-VA'}\right)\epsilon + \epsilon^{3/2}\lambda A = 0 , \tag{34}$$

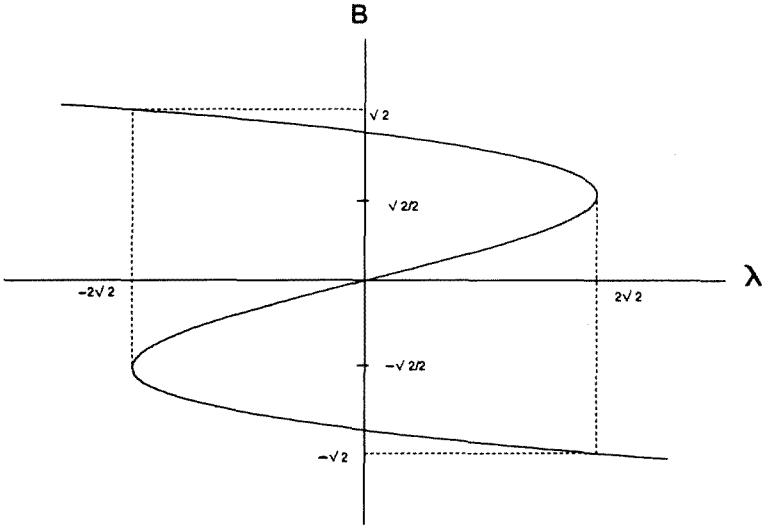


Fig. 5. A graph of $B$ against $\lambda$ obtained from eq. (31) showing the region of multiple solutions.

$$\frac{9}{64}(A+B)+\frac{3}{4}\left(AB+B^2+\frac{3}{16}\right)\epsilon^{1/2}$$
$$+\left(AB^2+\frac{9}{4}B-\frac{\lambda}{4}+B''+VB'\right)\epsilon-\epsilon^{3/2}\left(\lambda B-\frac{9}{4}\right)-\epsilon^2\lambda=0\,, \tag{35}$$

where primes now denote differentiation with respect to $\zeta$.

We now look for a solution of eqs. (34), (35) by expanding

$$A=A_0+\epsilon^{1/2}A_1+\epsilon A_2+\dots\,,$$

$$B=B_0+\epsilon^{1/2}B_1+\epsilon B_2+\dots\,,$$

$$V=V_0+\epsilon^{1/2}V_1+\dots\,. \tag{36}$$

At leading order we obtain

$$A_0+B_0=0 \tag{37}$$

and, on using (37), at $O(\epsilon^{1/2})$

$$A_1+B_1+1=0\,. \tag{38}$$

At $O(\epsilon)$ we obtain, on using expressions (37), (38),

$$\frac{9}{16}(A_2+B_2)=-\delta B_0''-V_0B_0'+B_0^3-\frac{3}{2}B_0+\frac{\lambda}{4} \tag{39}$$

from eq. (34) and

$$\frac{9}{64}(A_2+B_2)=-B_0''-V_0B_0'+B_0^3-\frac{3}{2}B_0+\frac{\lambda}{4} \tag{40}$$

from eq. (35). The compatibility equations (39), (40) then give the equation

$$(4-\delta)B_0''+3V_0B_0'-3\left(\frac{\lambda}{4}-\frac{3}{2}B_0+B_0^3\right)=0\,. \tag{41}$$

The reaction term in eq. (41) is the same as eq. (31) for the stationary states and the boundary conditions to be applied are that $B_0$ approaches one of the solutions of eq. (31) as $|\zeta|\to\infty$. It is readily established (using a similar argument to that given above for the case $\delta=1$) that eq. (41) does not admit pulse wave solutions (i.e. $B_0$ must attain different values as $\zeta\to\infty$ and as $\zeta\to-\infty$).

Clearly eq. (41) cannot have a solution which satisfies the required form for the boundary conditions when $\delta=4$. We can also establish that such a solution is also not feasible for $\delta>4$. To do so we linearize the equation about a (temporally stable) stationary state of the equation ($B_s$, say) putting $B_0=B_s+\beta$, where $\beta\ll B_s$. This results in the linear equation

$$(4-\delta)\beta'' + 3V_0\beta' - 9(B_s^2 - \tfrac{1}{2})\beta = 0\,. \tag{42}$$

Now, from Fig. 5 we can see that the term $(B_s^2 - \frac{1}{2}) > 0$ and using this, it is readily established that eq. (42) cannot have a solution (with $\delta > 4$) which approaches zero, and hence a solution in which $B_0$ approaches $B_s$, as both $\zeta \to \infty$ and as $\zeta \to -\infty$.

This suggests that for $\delta > 4$ simple autocatalytic front waves, in which the concentrations change monotonically from one (stable) state at their front to another (stable) state at their rear, will not be initiated and that a more complex wave structure may be expected. (This will be seen when we describe the results obtained from numerical integrations of an initial-value problem described below.) This value for $\delta$, obtained from an analysis for $(\frac{1}{8} - \beta_0) \ll 1$ is in line with the value of $\delta_1$ already obtained for the case $\beta_0 = 0$, (the slight difference between the two values could well be accounted for by numerical errors). The (close) agreement between these two values also suggests (though we are unable to establish it rigorously) that $\delta_1 \simeq 4$ for general values of $\beta_0 < 1/8$.

Finally, we note that the stationary wave solutions of eq. (41), which differentiate between type I and type II waves, correspond to taking $\lambda = 0$, with $\mu_c$ then being given by

$$\mu_c \sim \tfrac{27}{64} - \tfrac{9}{4}\epsilon + O(\epsilon^2) \quad \text{as } \epsilon \to 0\,. \tag{43}$$

The curve given by (43) emerges from the hysteresis point and bisects the two curves bounding the region of multiple solutions given by expression (32).

We now examine the implications of our results for travelling waves by considering an initial-value problem.

## 4. Initial-value problem: Numerical solutions

Here we consider numerical solutions to an initial-value problem given by eqs. (5), (6) on $-\infty < x < \infty$, $t > 0$, subject to the initial conditions that

$$a = a_3, \quad b = b_3 \quad \text{for } -\infty < x < 0\,,$$

$$a = a_1, \quad b = b_1 \quad \text{for } 0 < x < \infty\,. \tag{44}$$

Thus type I waves will propagate forwards (i.e. in the direction of $x$ increasing) while type II waves will propagate backwards (into $x < 0$).

The numerical method uses to solve eqs. (5), (6) subject to (44) is based on the Crank–Nicolson method, with Newton-Raphson iteration being used to solve the nonlinear finite-difference equations that arise at each time step. The computations were performed on a sufficiently large domain to allow travelling waves of permanent form to be set up, this being monitored by calculating their wave speed and noting that it had reached to a constant value (to within the overall numerical accu-

racy). No-flux boundary conditions were applied at the ends of the computational domain. This method has already been used successfully on a series of similar initial-value problem, in, for example, [7,12,13].

We obtained numerical solutions for a range of values of $\delta$, $\mu$ and $\beta_0$, the results are displayed by plots of $x_w$ (the position of the wave) against $t$. We started with $\delta = 1$ where we have already identified values of $\mu_c$ that differentiate between type I and type II waves. For $\beta_0 = 0$, $\mu_c = 2/9$ and the initiation of type I waves for $\mu < \mu_c$ and type II waves for $\mu > \mu_c$ is confirmed by the results shown in Fig. 6(a). For $\beta_0 = 0.05$, $\mu_c = 0.2858$ and again we can see (Fig. 6(b)) the existence of both type I

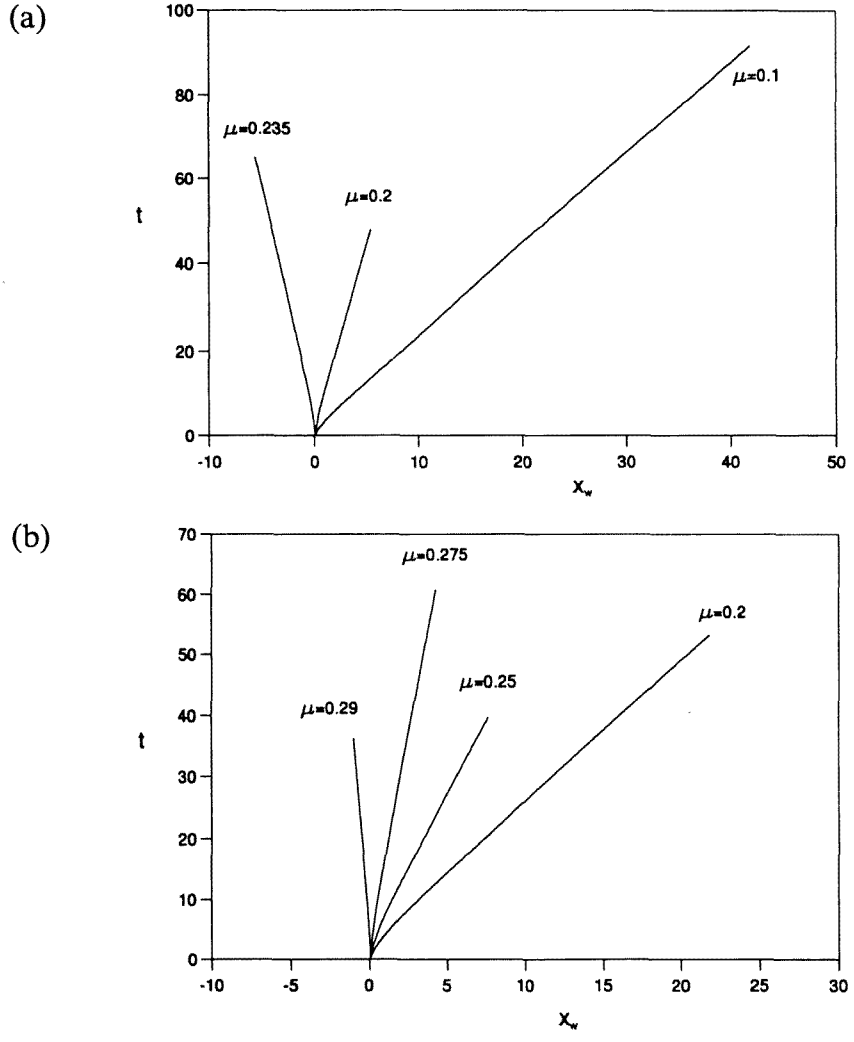


Fig. 6. Plots of wave position $x_w$ against $t$ for $\delta = 1.0$ and a range of values of $\mu$ with (a) $\beta_0 = 0.0$, (b) $\beta_0 = 0.05$.

and type II waves in the appropriate ranges of $\mu$. A typical wave profile (plotted after it had reached permanent form) (for $\beta_0 = 0.0, \mu = 0.1$) is shown in Fig. 7(a). A similar situation holds for $\delta < 1$ as can be seen in Fig. 8, where we plot $x_w \sim t$ for various values of $\mu$ and for $\delta = 0.2$, $\beta_0 = 0.0$ and $\beta_0 = 0.05$. A typical wave profile for $\delta = 0.2$, $\beta_0 = 0.05$, $\mu = 0.2$ is shown in Fig. 7(b). All the wave forms for $\delta < \delta_1$ appear to have the simple structure illustrated in Fig. 7, with monotone variations in the concentrations between the stable stationary states at the front and rear of the waves.

When we consider values $\delta > \delta_1$, as are illustrated in Figs. 9(a), 9(b) for $\delta = 5.0$,

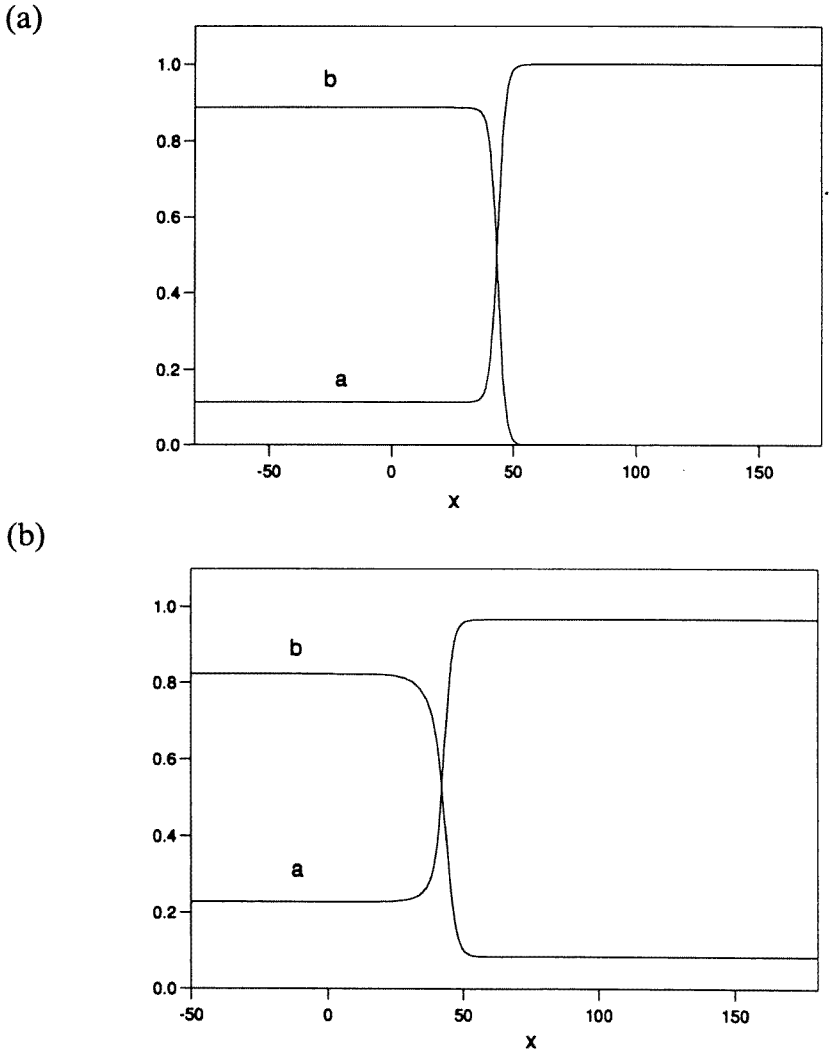


Fig. 7. Asymptotic wave profiles obtained from numerical integrations of the initial-value problem for (a) $\delta = 1.0, \beta_0 = 0.0, \mu = 0.1$, (b) $\delta = 0.2, \beta_0 = 0.05, \mu = 0.2$.

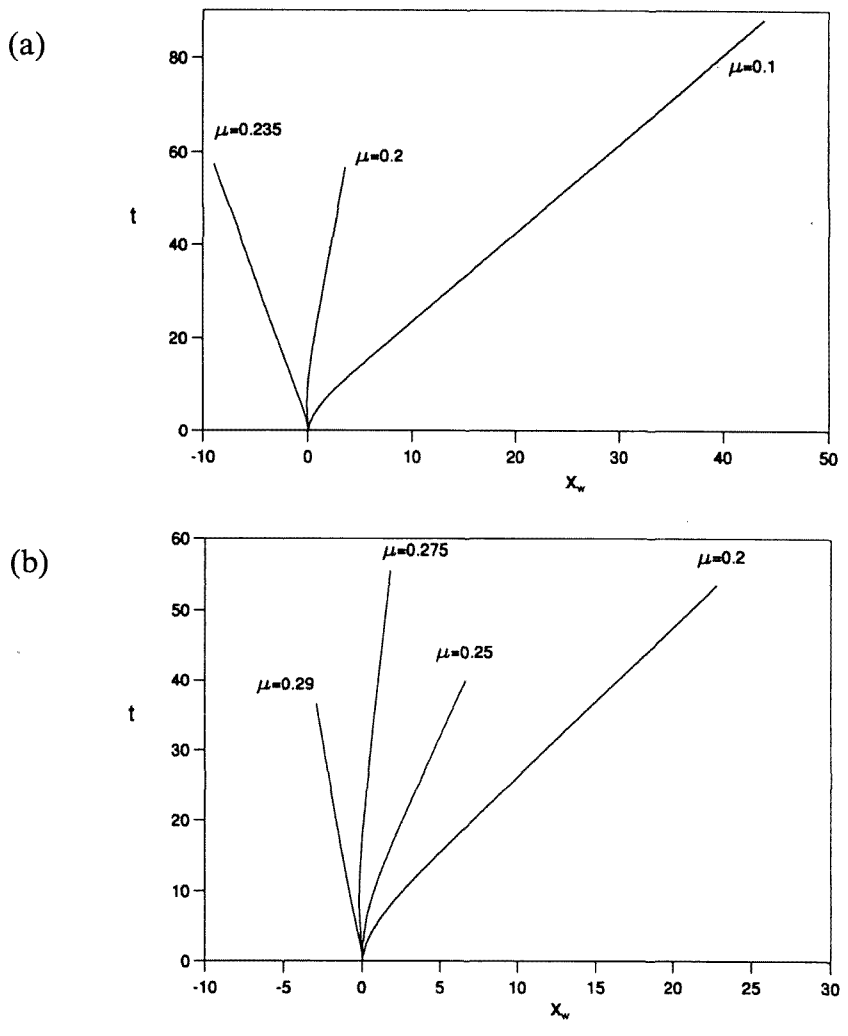


Fig. 8. Plots of wave position $x_w$ against $t$ for $\delta = 0.2$ and a range of values of $\mu$ with (a) $\beta_0 = 0.0$, (b) $\beta_0 = 0.05$.

we find that there is still a propagating front, though now only type I waves (i.e. propagation in the positive $x$-direction) being initiated. The velocity of these waves quickly approaches a constant value and in this respect they are similar to the waves seen for $\delta < \delta_1$. However, when we examine their wave structure in more detail (as in Fig. 9(c) for $\mu = 0.235$, $\delta = 5.0$, $\beta_0 = 0.0$, plotted at $t = 450$) a more complex behaviour is observed. Now the wave profiles are no longer monotone, with the concentrations undergoing oscillatory responses in the region behind the propagating front, with this region of oscillatory behaviour expanding backwards into the region $x < 0$. These oscillations in the concentration profiles are not especially

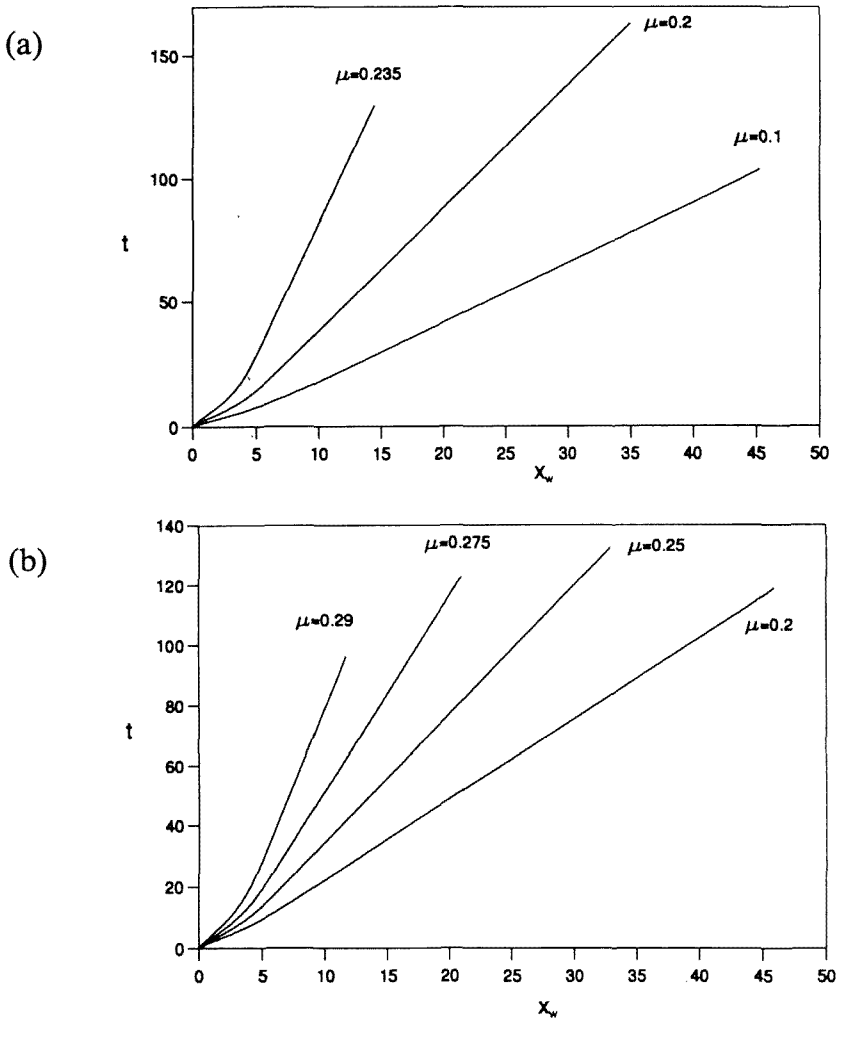


Fig. 9. Plots of wave position $x_w$ against $t$ for $\delta = 5.0$ and a range of values of $\mu$ with (a) $\beta_0 = 0.0$, (b) $\beta_0 = 0.05$, (c) wave profiles at large time ($t = 450$) for $\delta = 5.0, \beta_0 = 0.0, \mu = 0.235$.

marked for $\delta = 5$ (a value close to $\delta_1 \simeq 4$) but become much more pronounced for larger values of $\delta$, as can be seen in Fig. 10, (for $\delta = 50.0$) where we show wave profiles plotted at large times for $\mu = 0.2$ and $\beta_0 = 0.0$ (Fig. 10(a)) and $\beta_0 = 0.05$ (Fig. 10(b)). These figures clearly show the existence of a region behind the forward-propagating front where both concentrations $a$ and $b$ have an oscillatory behaviour. The oscillations in $a$ and especially in $b$ can be large with values of $b$ attained in the wave being more than double the stationary state values at the rear of the wave.

(c)

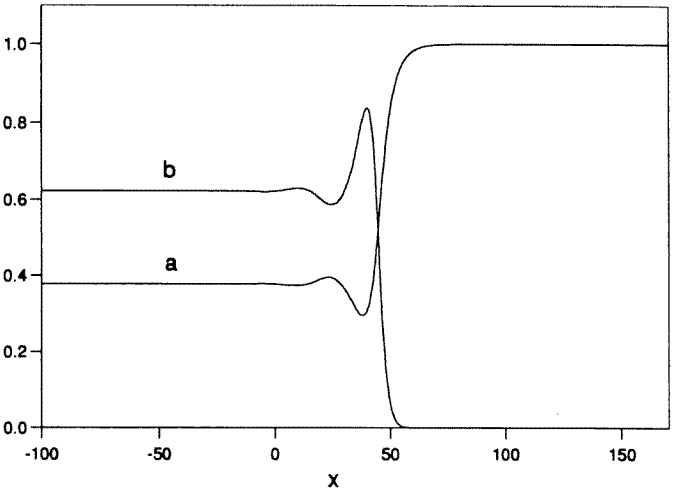


Fig. 9. (Continued.)

The expansion of this oscillatory region back into $x < 0$ can be seen in Fig. 11, where we give grey-level concentration plots of $b$ for the two cases taken for Fig. 10. These figures show the forward-propagating front (seen as the light-shaded line with positive slope) with this rapidly attaining a constant velocity. However, it is the structure at the rear of this front that is of most interest. Here we see the spatial oscillations in the concentration being formed and that these remain stationary with each individual peak response (say) remaining fixed in space after it has been formed. The whole region where this oscillatory behaviour is initiated can be observed propagating backwards into the region where $b = b_3$ (and temporally stable) creating (with the forward-propagating front) an expanding region of oscillatory response. The spatial oscillations in concentrations behind the front take a simple form after the initial transient period of their formation. We did not find more complex oscillatory behaviour in any of our numerical integrations (for cases not reported here) through these oscillations were seen for a wide range of values of the parameters and appear to be a generic feature of our reaction-diffusion system, as does the stationary nature of the individual oscillations.

The development of these standing waves in our model is related to Turing (or diffusion-drive instability), see, for example, Murray [14], whereby an otherwise stable, spatially uniform stationary state can become unstable if the diffusion coefficient of the autocatalyst (or activator species) is much less than that of the substrate (or inhibitor species), as is the case here. This aspect will be explored in more detail in a subsequent paper.

Finally, we undertook an extensive numerical investigation of our initial-value problem, with boundary conditions (44) ammended appropriately, to see if we could trigger pulse waves. We were unable to initiate any of these waves numeri-

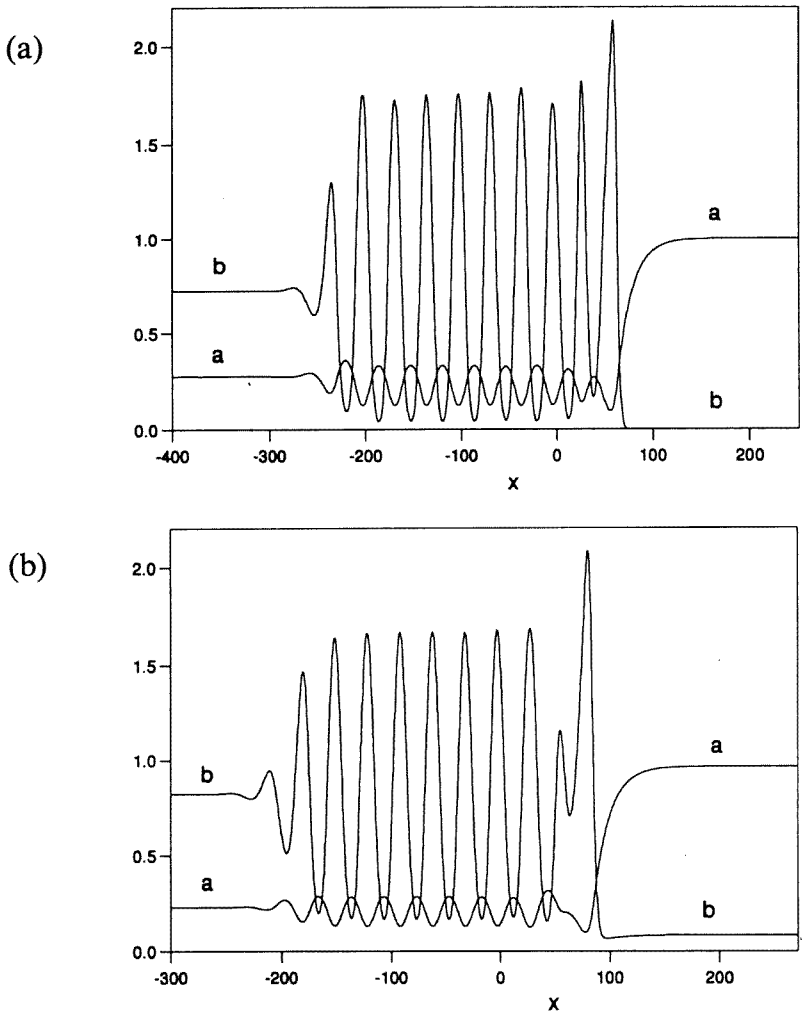


Fig. 10. Wave profiles obtained from numerical integrations of the initial-value problem plotted at large time for $\delta = 5.0$, $\mu = 0.2$ and (a) $\beta_0 = 0.0$, (b) $\beta_0 = 0.05$.

cally and as we have also been able to establish that pulse waves cannot occur for various limiting values of the parameters we may conclude that such waves appear not to be generated in this system (or if they are then only over a very restricted parameter range).

## 5. Conclusion

We have considered a model for a CFUR in which the reaction is given purely

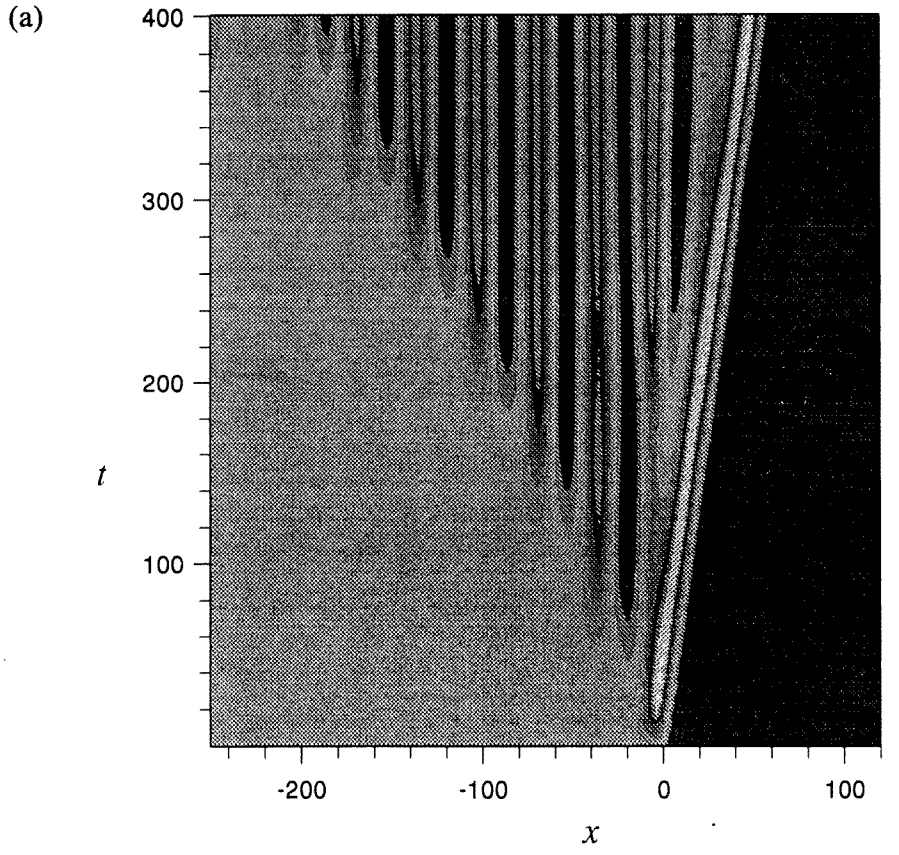


Fig. 11. Grey-level plots of $b$ for $\delta = 50.0$, $\mu = 0.2$ and (a) $\beta_0 = 0.0$, (b) $\beta_0 = 0.05$. In these figures the darker the value, the smaller the value of $b$.

by cubic autocatalysis and in which the exchange of reactants between the reactor and its environment is modelled by a diffusive interchange with the same mass transfer coefficient for both reactant $A$ and autocatalyst $B$. We have seen that this system is capable of supporting two, stable, spatially uniform stationary states. We have examined the possibility of initiating reaction-diffusion travelling waves of permanent form in this model for a CFUR and found that it is possible to do so provided the parameter $\delta$ (the ratio of the diffusion coefficients of $A$ and $B$) is sufficiently small. A value $\delta_1$, such that permanent form travelling waves can be formed for $\delta < \delta_1$, has been identified and our calculations suggest $\delta_1 \simeq 4$. This was confirmed by our numerical integrations of an initial-value problem.

For values of $\delta > \delta_1$ (i.e. $D_A \gtrsim 4D_B$) travelling waves of permanent form do not evolve as the large time structures to our initial-value problem, with now more complex waves structure being initiated. The main (and novel) feature of this structure is the region in which spatial oscillations in the concentrations of both reactant $A$

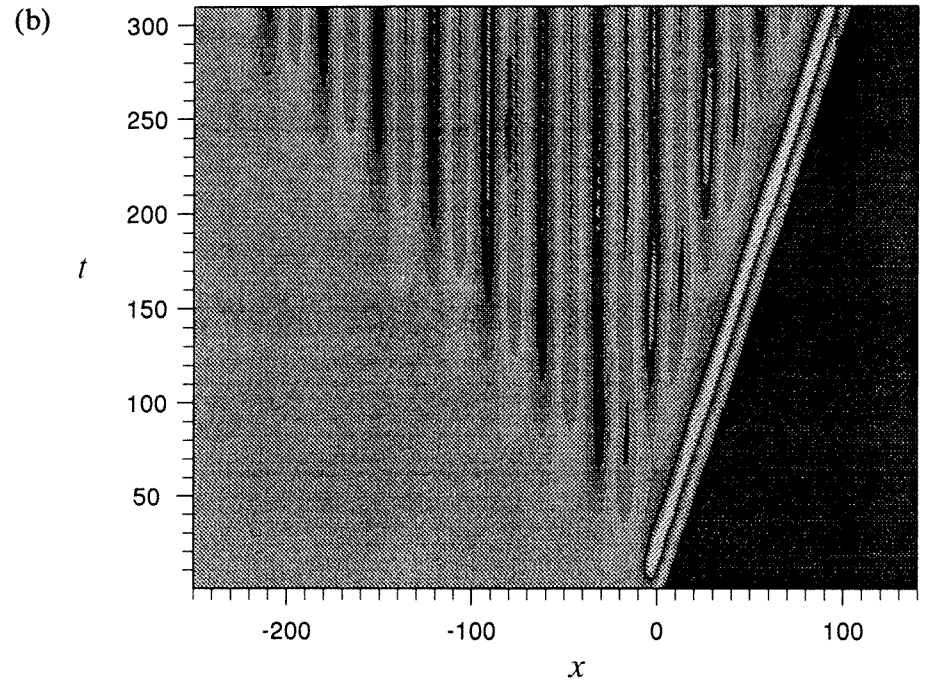


Fig. 11. (Continued.)

and autocatalyst $B$ are set up. These individual oscillations are of simple form and remain stationary in space but the region of the oscillatory response expands backwards at the rear of the forward-propagating front.

This feature, whereby stationary longitudinal oscillations in concentration are formed at the rear of a propagating front, is apparently new to reaction-diffusion systems with simple autocatalytic kinetics. It appears to be different to the transverse instabilities, leading to transverse oscillations in concentration, which have been predicted theoretically [15] for cubic autocatalysis and confirmed experimentally for the iodate-arsenous acid reaction [16]. There are several differences between the present case and these transverse oscillations, the main one being that the transverse oscillations in concentration are stationary relative to the propagating front, which suggests they are generated by a different mechanism. The only real similarity with the present case is that a value of $\delta > 1$ is required in both cases. Very recently Davidson et al. [17,18] have observed the occurrence of stationary spatial oscillations in a reaction-diffusion model for the spread of fungal mycelia. Their model has many similarities with the present model, as given by eqs. (2), (3) or (5), (6), and they also report that complex stationary spatial structures (their numerical results are obtained for two-dimensional geometry) are formed provided the ratio of the diffusion coefficients of the substrate and activator is sufficiently large.

## References

[1] J.E. Pearson, Science 261 (1993) 189.
[2] W.N. Reynolds, J.E. Pearson and S. Ponce-Dawson, Phys. Rev. Lett. 72 (1994) 2797.
[3] K.-J. Lee, W.D. McCormick, J.E. Pearson and H.L. Swinney, Nature 369 (1994) 215.
[4] V. Petrov, S.K. Scott and K. Showalter, Phil. Trans. R. Soc. Lond. A 347 (1994) 631.
[5] J.H. Merkin, V. Petrov, S.K. Scott and K. Showalter, Phys. Rev. Lett. 76 (1996) 546.
[6] J.H. Merkin, V. Petrov, S.K. Scott and K. Showalter, J. Chem. Soc. Faraday Trans. 92 (1996) 2911.
[7] J.H. Merkin and M.A. Sadiq, The propagation of travelling waves in an open cubic autocatalytic chemical system, accepted for publication in IMA Jl. Applied Math.
[8] P. Gray and S.K. Scott, *Chemical Oscillations and Instabilities* (Oxford University Press, 1990).
[9] A. Saul and K. Showalter, Propagating reaction-diffusion fronts, in: *Oscillations and Traveling Waves in Chemical Systems*, eds. R.J. Field and M. Burger (Wiley-Interscience, New York, 1984).
[10] J. Billingham and D.J. Needham, Phil. Trans. R. Soc. Lond. A 334 (1991) 1.
[11] J. Billingham and D.J. Needham, Dynamics and Stability of Syst. 6 (1991) 33.
[12] J.H. Merkin and D.J. Needham, J. Eng. Math. 23 (1989) 343.
[13] D.J. Needham and J.H. Merkin, Nonlinearity 5 (1992) 413.
[14] J.D. Murray, *Mathematical Biology* (Springer, Berlin, 1990).
[15] D. Horvath, V. Petrov, S.K. Scott and K. Showalter, J. Chem. Phys. 98 (1993) 6332.
[16] D. Horvath and K. Showalter, J. Chem. Phys. 102 (1995) 2471.
[17] F.A. Davidson, B.D. Sleeman, A.D.M. Rayner, J.W. Crawford and K. Ritz, Large-scale behaviour of fungal mycelia, to appear in Math. Comput. Modelling.
[18] F.A. Davidson, B.D. Sleeman, A.D.M. Rayner, J.W. Crawford and K. Ritz, Proc. R. Soc. Lond. B263 (1996) 873.